


Using G_0W_0 Level Alignment to Identify Catechol's Structure on $\text{TiO}_2(110)$

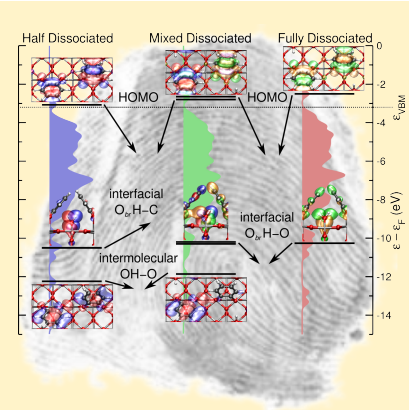
Duncan J. Mowbray^{*,†} and Annapaola Migani^{*,‡}

[†]Nano-Bio Spectroscopy Group and ETSF Scientific Development Center, Departamento de Física de Materiales, Universidad del País Vasco UPV/EHU and DIPIC, E-20018 San Sebastián, Spain

[‡]Catalan Institute of Nanoscience and Nanotechnology (ICN2), CSIC and The Barcelona Institute of Science and Technology, Campus UAB, Bellaterra, E-08193 Barcelona, Spain

 Supporting Information

ABSTRACT: We perform state-of-the-art calculations for a prototypical dye sensitized solar cell: catechol on rutile $\text{TiO}_2(110)$. Catechol is often used as an anchoring group for larger more complex organic and inorganic dyes on TiO_2 and forms a type II heterojunctions on $\text{TiO}_2(110)$. In particular, we compare quasiparticle (QP) G_0W_0 with hybrid exchange correlation functional (HSE) density functional theory (DFT) calculations for the catechol-rutile $\text{TiO}_2(110)$ interface. In so doing, we provide a theoretical interpretation of ultraviolet photoemission spectroscopy (UPS) and inverse photoemission spectroscopy (IPES) experiments for this prototypical system. Specifically, we demonstrate that the position, presence, and intensity of peaks associated with catechol's HOMO, intermolecular OH-O bonds, and interfacial hydrogen bonds to the surface bridging O atoms ($\text{O}_{br}\text{-H-C}$ and $\text{O}_{br}\text{-H-O}$) may be used to fingerprint deprotonation of catechol's OH anchoring groups. Furthermore, our results suggest deprotonation of these groups, while being nearly isoenergetic at high coverages, may significantly increase the photovoltaic efficiency of catechol- $\text{TiO}_2(110)$ interfaces.



1. INTRODUCTION

Catechol on $\text{TiO}_2(110)$ is a prototypical system for modelling industrially relevant dye sensitized solar cells.¹⁻⁷ This is for two reasons. (1) Catechol is often used as an anchoring group⁸ for larger more complex organic and inorganic dyes. (2) Catechol forms type II heterojunctions,⁸ where the dye's highest occupied molecular orbital (HOMO) is a gap state, while the lowest unoccupied molecular orbital (LUMO) is above the conduction band minimum (CBM) of the substrate, e.g., TiO_2 . The level alignment for this system has previously been studied experimentally via ultraviolet photoemission spectroscopy (UPS)^{1,9} and inverse photoemission spectroscopy (IPES),⁹ and thus provides an excellent benchmark type II system to be studied theoretically using many-body quasiparticle (QP) techniques, such as G_0W_0 .¹⁰⁻¹² For such type II systems, the HOMO-LUMO and HOMO-CBM separations determine the onset of the absorption spectra. In such photovoltaic devices, the dye's role is to reduce the onset of the absorption spectra to sub-band gap energies, and maximize the overlap with the solar spectrum.^{5,13}

The exact structure of the catechol-rutile $\text{TiO}_2(110)$ interface is difficult to identify and control experimentally. This is because for hydroxylated molecules such as catechol, a complex network of interfacial and intermolecular bonds is formed upon adsorption. Moreover, catechol's anchoring OH groups can be either fully dissociated, partially dissociated, or intact, with each catechol overlayer having similar adsorption energies. Still, dissociation plays a significant role in determining the level alignment^{1,14} and, hence, the photovoltaic efficiency¹³ of the interface.

Generally, the HOMO moves to higher energy upon deprotonation for hydroxylated molecules, e.g., CH_3OH on $\text{TiO}_2(110)$ ¹⁵ and

H_2O on rutile $\text{TiO}_2(110)$ ¹⁶ and anatase $\text{TiO}_2(101)$.¹⁷ For this reason, the HOMO's energy provides a fingerprint of the interface's structure. This is augmented by the presence of distinct identifiable levels associated with intermolecular and interfacial OH-O hydrogen bonds. Specifically, the hydrogenated bridging O atoms (HO_{br}) resulting from interfacial deprotonation of the anchoring groups are consistently at ~ 10 eV below the Fermi level ϵ_F on $\text{TiO}_2(110)$.^{14,16,18,19}

To describe both highly hybridized¹⁶ and localized^{15,20} molecular interfacial levels, one requires a correct description of the anisotropic screening, i.e., electron-electron interaction, at the interface. This is clearly seen from the level alignment of H_2O on $\text{TiO}_2(110)$.¹⁶

On the one hand, H_2O 's $1b_1$ level becomes highly hybridized with the substrate upon adsorption on $\text{TiO}_2(110)$.¹⁶ The interfacial level alignment of these highly hybridized levels with the substrate VBM is already described by density functional theory (DFT). This is because the screening of these levels is essentially the dielectric constant of the substrate. At the G_0W_0 level, the DFT Kohn-Sham (KS) eigenenergies are shifted by Δ , the difference between the QP self-energy ($\Sigma = iG_0W_0$) and the xc potential (V_{xc}), up to a normalization factor Z , i.e., $\Delta \equiv Z(\Sigma - V_{xc})$.¹² For example, $\Delta \approx 0.1$ and 0.7 eV for all levels of the $\text{TiO}_2(110)$ substrate from G_0W_0 based on DFT calculations employing a generalized gradient approximation (PBE)²¹ and a hybrid range separated (HSE)²² exchange and correlation (xc)-functional, respectively.²³

On the other hand, H_2O 's $3a_1$ and $1b_2$ levels remain mostly localized on the molecule upon adsorption on $\text{TiO}_2(110)$.¹⁶ The alignment of these localized levels, whose screening is significantly different from that of the substrate, is poorly described at

the DFT level. Not even HSE²² provides an accurate description of the interfacial level alignment for localized levels, e.g., H₂O's 3a₁ and 1b₂ and CH₃OH's a'' on TiO₂(110).^{16,23} This is because HSE DFT calculations effectively perform a constant static screening of the exchange term, i.e., the fraction of Hartree-Fock exact-exchange included $\alpha = 0.25$ is effectively an inverse dielectric constant $\alpha \approx \epsilon_{\infty}^{-1}$.²⁴ For this reason, HSE performs well for systems with a homogeneous screening and $\epsilon_{\infty} \sim 4$.^{16,23,24}

To correctly account for differences in screening between the molecular layer and substrate, one may use many-body QP techniques, such as G_0W_0 .¹¹ In such methods, the spatial dependence of the screening is included explicitly. In fact, for occupied levels, Δ is linearly dependent on the fraction of the wave function's density within the molecular layer f_{mol} .^{15,23,25} This means by just rigidly shifting all the levels, one cannot describe the alignment of occupied levels with significant density outside the substrate.

For type I interfaces, i.e., H₂O or CH₃OH on TiO₂(110),^{15,16,20,23} we have previously demonstrated that G_0W_0 provides an accurate alignment for both localized and highly hybridized levels. In each case, G_0W_0 shifts the localized levels to stronger binding, into quantitative agreement with UPS experiments.

In this study, we compare the projected density of states (PDOS) onto catechol obtained from QP PBE G_0W_0 and HSE DFT calculations with the measured UPS and IPES spectra for the catechol-rutile TiO₂(110) interface. In so doing, this study provides a complete state-of-the-art computational description of the simplest experimentally relevant type II interface. Based on our analysis of the PDOS, we are able to suggest the most likely structure of the catechol overlayer measured in UPS experiments. In fact, our results suggest the degree of catechol dissociation may differ with the experimental conditions employed.^{1,9} Our results suggest fully deprotonating the anchor groups of the overlayer should lead to an increased efficiency of the photovoltaic device.

2. METHODOLOGY

Our G_0W_0 calculations^{10–12} have been performed using VASP within the projector augmented wave (PAW) scheme.²⁶ The G_0W_0 calculations are based on KS wave functions and eigenenergies from DFT obtained using PBE.²¹ DFT calculations employing the HSE06 variant²² of the HSE xc-functional have been carried out for comparison with PBE G_0W_0 calculations.

In the G_0W_0 approach, the contribution to the KS eigenvalues from the xc-potential V_{xc} is replaced by the QP self energy $\Sigma = iG_0W_0$ in a single step, where G_0 is the Green's function and W_0 is the screening¹⁰ based on the KS wave functions and eigenvalues.¹¹ The dielectric function is obtained from linear response time-dependent (TD) DFT within the random phase approximation (RPA), including local field effects.¹² From G_0W_0 one obtains first-order QP corrections Δ to the KS eigenvalues, but retains the KS wave functions.

The geometries have been fully relaxed using the PBE²¹ xc-functional, with all forces $\lesssim 0.02$ eV/Å. We employ a plane-wave energy cutoff of 445 eV, an electronic temperature $k_B T \approx 0.2$ eV with all energies extrapolated to $T \rightarrow 0$ K, and a PAW pseudopotential for Ti which includes the 3s² and 3p⁶ semi-core levels. The calculations have been performed spin unpolarized. All unit cells contain a four layer TiO₂(110) slab, employ the measured lattice parameters of bulk rutile TiO₂ ($a = 4.5941$ Å, $c = 2.958$ Å),²⁷ and include at least 27 Å of vacuum between repeated images. In each case, equivalent catechol overlayers are adsorbed on both sides of the slab. We employ Γ centered k -point meshes with densities $\Delta k < 0.25$ Å⁻¹, approximately 9% unoccupied bands per atom, i.e. including all levels up to 30 eV above the VBM, an energy cutoff

of 80 eV for the number of \mathbf{G} -vectors, and a sampling of 80 frequency points for the dielectric function. The G_0W_0 parameters are consistent with those previously used for describing both rutile and anatase TiO₂ bulk, rutile TiO₂(110) and anatase TiO₂(101) clean surfaces, and their interfaces.^{15–17,23} These parameters have been shown to provide accurate descriptions of bulk rutile and anatase optical absorption spectra, and both clean surface and interfacial level alignment.^{15–17,23}

The adsorption energy E_{ads} of catechol on Ti coordinately unsaturated (Ti_{cus}) sites of a TiO₂(110) surface is given by

$$E_{ads} \approx \frac{E[n\text{Catechol} + \text{TiO}_2(110)] - E[\text{TiO}_2(110)]}{n} - E[\text{Catechol}], \quad (1)$$

where n is the number of adsorbed catechol molecules in the supercell, and $E[n\text{Catechol} + \text{TiO}_2(110)]$, $E[\text{TiO}_2(110)]$, and $E[\text{Catechol}]$ are the total energies of the covered and clean surfaces and gas phase catechol molecule, respectively. For catechol in the gas phase, we find the most stable conformation has an intramolecular hydrogen bond, i.e., C_s symmetry.

Scanning tunneling microscopy (STM) simulations have been performed using the Tersoff-Hamann approximation.²⁸ In this approach, the current I at a position \mathbf{r} is given by

$$I(\mathbf{r}) = C \int_{\epsilon_F}^{\epsilon_F + U} \rho(\mathbf{r}, \epsilon) d\epsilon \approx C U \rho(\mathbf{r}, \epsilon_F) \approx C U \rho(\mathbf{r}, \epsilon_F + U), \quad (2)$$

where C is a prefactor which depends on the DOS, surface work function, and tip radius. U is the potential of the sample relative to the tip in the experiment, i.e., the applied potential relative to the experimental Fermi level ϵ_F . $\rho(\mathbf{r}, \epsilon)$ is the local DOS, given by

$$\rho(\mathbf{r}, \epsilon) = \sum_{n\mathbf{k}} \delta(\epsilon_{n\mathbf{k}} - \epsilon) \frac{|\psi_{n\mathbf{k}}(\mathbf{r})|^2}{N_{\mathbf{k}}} \approx \sum_{n\mathbf{k}} \exp \left[- \left(\frac{\epsilon_{n\mathbf{k}} - \epsilon}{k_B T} \right)^2 \right] \frac{|\psi_{n\mathbf{k}}(\mathbf{r})|^2}{N_{\mathbf{k}}}, \quad (3)$$

where $\epsilon_{n\mathbf{k}}$ is the G_0W_0 eigenvalue and $\psi_{n\mathbf{k}}$ is the KS wave function of level n at k -point \mathbf{k} , $k_B T \approx 0.2$ eV is the electronic temperature of the calculation, and $N_{\mathbf{k}}$ is the weight of k -point \mathbf{k} . To emphasize any dependence of $I(\mathbf{r})$ on the applied bias U , we have used throughout $I(\mathbf{r}) \approx C U \rho(\mathbf{r}, \epsilon_F + U)$. It should be noted, however, that similar results are obtained by integrating ρ over the bias window $[\epsilon_F, \epsilon_F + U]$ (see Figure S1 in Supporting Information). Herein, ρ is plotted at an isosurface value of 5×10^{-8} e/Å³. This is somewhat greater than its maximum far from the surface, i.e.,

$$\min_z \left(\max_{x,y} \rho(x, y, z; \epsilon_F + U) \right) < 5 \times 10^{-8} \text{ e/Å}^3. \quad (4)$$

This ensures ρ is defined at this isosurface value throughout the surface plane.

Experimental spectra are typically referred to the Fermi level, ϵ_F , which is pinned ~ 0.1 eV below the CBM for mildly reduced TiO₂.^{29–31} Using the electronic band gap for rutile TiO₂ of 3.3 ± 0.5 eV obtained from electron spectroscopy measurements,³² the experimental VBM energy relative to the Fermi level is $\epsilon_{VBM} \approx 0.1 - 3.3 \approx -3.2$ eV.²³ Since the VBM is the most reliable theoretical energy reference,²³ we subtract $\epsilon_{VBM} \approx -3.2$ eV from the measured UPS and IPES spectra to align with the calculated G_0W_0 DOS and PDOS, and vice versa.

We align the DOS and PDOS with respect to the deepest Ti semi-core level (3s²). This allows a direct comparison between spectra for half (½D ½D), mixed (D ½D), and fully (D D) dissociated catechol overlayers. In each case, the highest occupied levels belong to the catechol overlayer. As we are interested in seeing the difference between the HOMO position and the TiO₂(110) VBM for each catechol overlayer, the highest occupied level is not a good reference.

Moreover, the catechol anchor groups form Ti_{cus}–O bonds, mak-

ing it impractical to separate the O $2p\pi$ surface levels from those of the molecule. This makes it difficult to identify a highest occupied level with purely surface contributions, which can be associated with the clean surface's VBM. For this reason, one should use the Ti levels as reference, e.g., occupied semi-core Ti $3s^2$ or unoccupied Ti $3d$ CBM levels. Here, we align with respect to the deepest semi-core Ti $3s^2$ levels. In this way we obtain a consistent alignment relative to the surface levels for each configurations. We find this is effectively equivalent to aligning relative to the TiO_2 CBM, i.e., Ti $3d$ levels.

Using the semi-core levels, we remove differences in work function between surfaces, which would be present if the vacuum level were used as a reference. Here, we take the energy of the VBM for the clean surface $\varepsilon_{\text{VBM}}^{\text{clean}}$ relative to its deepest Ti $3s^2$ semi-core level $\varepsilon_{\text{Ti}3s^2}^{\text{clean}}$ as our final reference relative to the catechol interface's deepest Ti $3s^2$ level $\varepsilon_{\text{Ti}3s^2}$. More precisely, $\varepsilon_{\text{VBM}} = \varepsilon_{\text{VBM}}^{\text{clean}} - \varepsilon_{\text{Ti}3s^2}^{\text{clean}} + \varepsilon_{\text{Ti}3s^2}$, in Figures 3 and 4.

However, for reduced $\text{TiO}_{2-x}(110)$, where Ti $3d$ levels are occupied, all the Ti levels are consequently upshifted compared to stoichiometric $\text{TiO}_2(110)$. This makes the Ti levels a poor reference for comparison between such systems. For this reason, we use the VBM as an energy reference for 1 ML H@O_{br} on $\text{TiO}_2(110)$, as it is a type I interface.

3. RESULTS AND DISCUSSION

Catechol consists of a benzene ring with two adjacent anchoring OH groups. It has been previously shown, both theoretically and experimentally, that catechol adsorbs on the Ti_{cus} sites of the rutile $\text{TiO}_2(110)$ surface via the OH anchor groups in a bidentate configuration.

At low coverage, catechol preferentially adsorbs upright ($\theta \approx 86^\circ$) on the surface, parallel to the $[001]$ c -axis,² with both anchoring groups deprotonated, i.e., fully dissociated, with an accompanying charge of $-0.4e$ transferred to the nearest O_{br} atom of the $\text{TiO}_2(110)$ surface. As the coverage increases ($\sim 2/3$ ML), catechol tilts ($\theta \sim 67^\circ$) toward the surface, with two interfacial $\text{O}_{br}\text{H}-\text{O}$ bonds (cf. Table 1).

Table 1. Adsorption Energies E_{ads} in Electronvolts per Molecule for $1/2$ ML 1×4 , $2/3$ ML 1×3 , and 1 ML 1×4 Intact (I), Half ($1/2$ D) and Fully (D) Dissociated Catechol Overlayers on $\text{TiO}_2(110)$ with Tilting Angle θ in Degrees and Number of Interfacial (OH-O) and Intermolecular (OH-O, $\text{O}_{br}\text{H}-\text{C}$, and $\text{O}_{br}\text{H}-\text{O}$) Bonds per Unit Cell

structure (ML)	θ ($^\circ$)	OH-O	OH- O_{br} (bonds/unit cell)	$\text{O}_{br}\text{H}-\text{C}$	$\text{O}_{br}\text{H}-\text{O}$	E_{ads} (eV)
$1/2$ D	86	0	0	0	2	-0.792
I	87	0	0	0	0	-0.249
I	61	0	2	0	0	-0.595
$2/3$ $1/2$ D	80	0	1	0	1	-0.620
$2/3$ $1/2$ D	63	0	1	0	1	-0.676
D	78	0	0	2	0	-0.676
D	87	0	0	0	2	-0.705
D	67	0	0	0	2	-0.748
1 $1/2$ D $1/2$ D	56, 49	2	0	2	0	-0.614
1 $1/2$ D $1/2$ D	55, 48	1	1	0	2	-0.600
1 $1/2$ D $1/2$ D	54, 46	2	0	0	2	-0.598
1 D $1/2$ D	56, 48	1	0	1	2	-0.685
1 D $1/2$ D	56, 48	1	0	2	1	-0.653
1 D D	56, 49	0	0	2	2	-0.652

At high coverage (1 ML), where catechol molecules adsorb on every Ti_{cus} site, they are forced to tilt in alternating directions due to steric hindrance. This gives rise to the 1×4 catechol overlayers seen via STM¹ and shown in Figure 1. Further, at this coverage, besides interfacial hydrogen bonds to the surface HO_{br} , the overlayer, when not fully dissociated, is stabilized by intermolecular hydrogen bonds between neighboring catechol molecules. For this reason, the half, mixed, and fully dissociated catechol adsorption energies are all within 0.1 eV, i.e., the accuracy of DFT (cf. Ta-

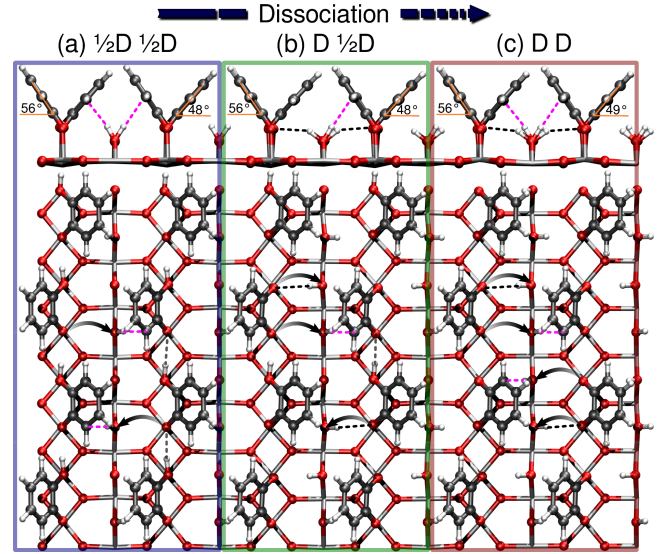


Figure 1. Schematics of 1 ML catechol adsorbed (a) half ($1/2$ D $1/2$ D, blue), (b) mixed (D $1/2$ D, green), and (c) fully (D D, red) dissociated on coordinately unsaturated Ti sites (Ti_{cus}) of $\text{TiO}_2(110)$. Charge transfer of $\sim -0.4e$ accompanying deprotonation is represented by arrows, while intermolecular OH-O (gray) and interfacial $\text{O}_{br}\text{H}-\text{O}$ (black) and $\text{O}_{br}\text{H}-\text{C}$ (magenta) hydrogen bonds are denoted by dotted lines. The angle between catechol's benzene ring and the surface plane, θ , is shown above.

ble 1). These results have also been reproduced to within 25 meV using the real space PAW DFT code GPAW.^{33,34}

Overall, we find catechol binds more weakly to the surface as the coverage increases. This is attributable to steric hindrance, especially for a 1 ML coverage. Furthermore, the binding energy at $2/3$ ML coverage is significantly stronger for deprotonated anchoring groups and tilted catechol molecules (cf. Table 1). This is consistent with previous DFT studies of catechol on $\text{TiO}_2(110)$.⁴

The most stable 1 ML half, mixed, and fully dissociated catechol overlayers listed in Table 1 are shown in Figure 1. The 1 ML $1/2$ D $1/2$ D structure (Figure 1(a)) has two intermolecular OH-O (gray dashed lines) and two interfacial $\text{O}_{br}\text{H}-\text{C}$ bonds (magenta dashed lines), the 1 ML D $1/2$ D structure (Figure 1(b)) has one intermolecular OH-O, one interfacial $\text{O}_{br}\text{H}-\text{C}$, and two interfacial $\text{O}_{br}\text{H}-\text{O}$ bonds (black dashed lines), while the 1 ML D D structure (Figure 1(c)) has two interfacial $\text{O}_{br}\text{H}-\text{C}$ and two interfacial $\text{O}_{br}\text{H}-\text{O}$ bonds. In each case, interfacial deprotonation of the anchoring OH groups is accompanied by a charge transfer of $-0.4e$ to the nearest O_{br} atom, as depicted schematically in Figure 1. Such intermolecular and interfacial hydrogen bonding combinations have also been reported for the 1 ML methanol- $\text{TiO}_2(110)$ interface.^{15,35} Figure 1 shows that the two tilting directions are inequivalent, with adjacent catechols tilted by $\theta \sim 56^\circ$ and 48° . For the $\text{O}_{br}\text{H}-\text{O}$ interfacial hydrogen bonds, catechol tilts away from the O_{br}H moiety, while for the $\text{O}_{br}\text{H}-\text{C}$ interfacial hydrogen bonds, catechol tilts towards the O_{br}H moiety. For the latter, the $\text{O}_{br}\text{H}-\text{C}$ bond is mostly HO_{br} σ in character, with a minor C $2p\pi$ contribution from the neighboring C atoms.

STM images of the 1×4 catechol overlayer,¹ and simulated images for the $1/2$ D $1/2$ D, D $1/2$ D, and D D structures are shown in Figure 2. In order to reproduce the line scan's minima, i.e., effective height, it is necessary to perform the line scan along the $[\bar{1}11]$ direction, as indicated by arrows in Figure 2(a-f). This is particularly important for the D D structure, where a line scan along the $[\bar{1}11]$ direction would not cross the computed STM minima. Comparing the measured and computed line scans along the $[\bar{1}11]$ direction, we thus conclude that the measured catechol overlayer is the mirror

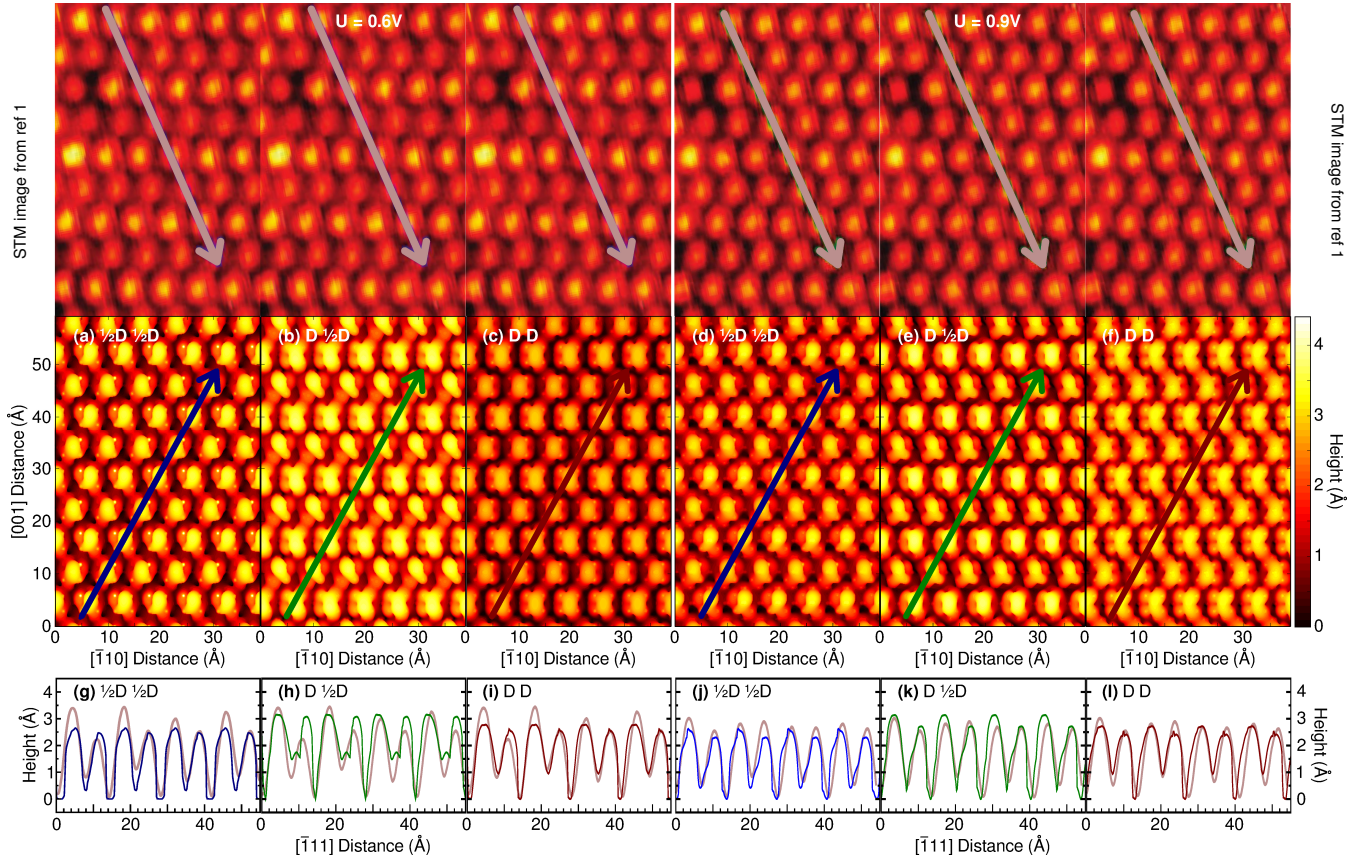


Figure 2. Constant current (a–f) STM and (g–l) line scans at (left panels) $U = 0.6$ V and (right panels) $U = 0.9$ V from ref 1 (upper panels and brown thick lines) and calculated LDOS (lower panels and blue/green/red thin lines) for (a,d,g,j) half ($\frac{1}{2}$ D $\frac{1}{2}$ D, blue), (b,e,h,k) mixed (D $\frac{1}{2}$ D, green), and (c,f,i,l) fully (D D, red) dissociated catechol overlayers on $\text{TiO}_2(110)$ at $5 \times 10^{-8} e/\text{\AA}^3$. Heights in Å are relative to the measured or calculated minimum.

image of the computed structures shown in Figure 1.

Overall, the average heights h from line scans and simulated STM images agree qualitatively for all three computed structures at both $U = 0.6$ V ($h \approx 2.79$ Å, $h_{\text{exp}} \approx 2.87$ Å) and $U = 0.9$ V ($h \approx 2.67$ Å, $h_{\text{exp}} \approx 2.75$ Å). However, the difference in height between neighbouring molecules Δh is underestimated at $U = 0.6$ V ($\Delta h \approx 0.14$ Å, $\Delta h_{\text{exp}} \approx 0.81$ Å), but agrees qualitatively at $U = 0.9$ V ($\Delta h \approx 0.32$ Å, $\Delta h_{\text{exp}} \approx 0.22$ Å). Altogether, this indicates that the structure of the unoccupied levels at these biases are rather insensitive to the deprotonation of catechol’s anchoring OH groups. This is not surprising, considering the structural similarity of the benzene ring orientation for each type of overlayer shown in Figures 1 and 2.

In summary, STM provides direct information as to the relative orientation of catechol on the surface which forms the 1×4 overlayer on $\text{TiO}_2(110)$. However, STM lacks direct information about deprotonation of the OH anchor groups. Such information is important, as it determines the relative level alignment of the molecule’s HOMO with the substrate’s VBM. To obtain direct information about the level alignment, one must compare the G_0W_0 PDOS with UPS and IPES spectra.

In Figure 3, we identify features of the G_0W_0 PDOS which may be used to fingerprint the catechol overlayer’s structure. These features are the HOMO, HOMO–1, interfacial HO_{br} , and intermolecular HO–O levels associated with the half (blue/red) and fully (green/orange) dissociated surface catechol species. Dotted lines connect energy levels associated with the half or fully dissociated catechol species.

Although catechol’s gas phase spectrum contains many additional occupied π and σ skeletal levels, shown in gray in Fig-

ure 3(a), these levels are rather insensitive to deprotonation of the OH anchor groups. For this reason, they are ineffective for distinguishing between $\frac{1}{2}$ D $\frac{1}{2}$ D, D $\frac{1}{2}$ D, and D D catechol overlayers on $\text{TiO}_2(110)$.

As a reference, the HOMO and HOMO–1 levels of gas phase catechol are depicted in Figure 3(a), aligned relative to the molecule’s HOMO. Figure 3(b), (c), and (d) show that the HOMO and HOMO–1 are pinned to each other, and shift up in energy with deprotonation of adsorbed catechol. This deprotonation of the OH anchor group induces a charge transfer of $\sim -0.4e$ to the substrate. As charge is removed from the molecule, the HOMO and HOMO–1 are destabilized. This effect is even more pronounced at the G_0W_0 level, as the molecule’s ability to screen the HOMO and HOMO–1 levels is also reduced as charge is transferred to the substrate.¹⁵ Consequently, the energy separation between HOMO and VBM may be used to distinguish between half, mixed, and fully dissociated catechol overlayers on $\text{TiO}_2(110)$.

Another fingerprint of dissociated catechol is the presence of HO_{br} surface levels at ~ 10 eV below the experimental Fermi level. The HO_{br} level is a general feature of all the interfaces formed from rutile $\text{TiO}_2(110)$ and hydroxylated molecules, e.g., H_2O and CH_3OH .¹⁶ As a reference, we show in Figure 3(e) both in and out of phase HO_{br} σ levels for 1 ML H@O_{br} on $\text{TiO}_2(110)$.¹⁶ This structure is equivalent to $\frac{1}{2}$ ML dissociated H_2O adsorbed on bridging O vacancies ($\text{H}_2\text{O@O}_{br}^{\text{vac}}$) of a reduced $\text{TiO}_{2-\frac{1}{4}}(110)$ surface.¹⁶ In Figure 3(c,d) we show HO_{br} levels associated with adjacent O_{br}H –O bonds, while for (b), we show O_{br}H –C levels. For this reason, the HO_{br} levels in (b) have less weight on the benzene ring compared to (c,d). Despite the differences in reduction of the

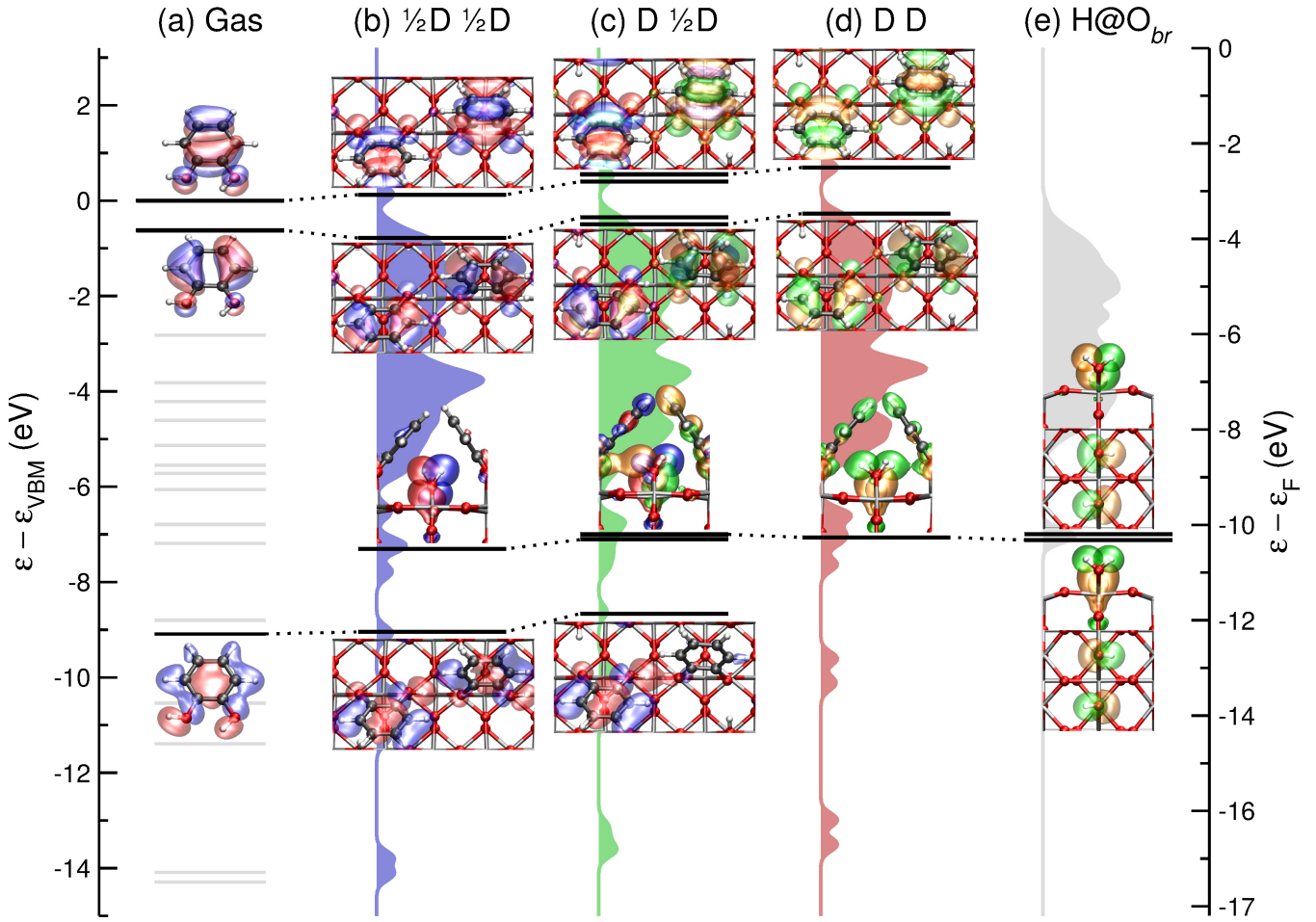


Figure 3. HOMO, HOMO-1, OH-O, and HO_{br} DFT orbitals and G_0W_0 eigenvalues and DOS for catechol (a) in the gas phase (grey lines), 1 ML (b) half ($\frac{1}{2}\text{D}$ $\frac{1}{2}\text{D}$, blue), (c) mixed (D $\frac{1}{2}\text{D}$, green), or (d) fully dissociated (D D, red), and (e) H@O_{br} (grey) on $\text{TiO}_2(110)$. (b,c,d) Colors are used to differentiate between $\frac{1}{2}\text{D}$ (red/blue) and D (orange/green) catechol orbitals. Energies are relative to the VBM (ϵ_{VBM}) of clean $\text{TiO}_2(110)$ (left) or the experimental Fermi level (right).

substrate between the systems depicted in Figures 3(b,c,d,e), the HO_{br} levels are surprisingly consistent in energy.

As can be seen in Figure 1(a), for $\frac{1}{2}\text{D}$ $\frac{1}{2}\text{D}$, the HO_{br} groups are on every other O_{br} , whereas in Figure 1(b,c), the HO_{br} -O bonds for D $\frac{1}{2}\text{D}$ and D D are on adjacent O_{br} . For this reason, the HO_{br} levels are essentially isoenergetic in Figure 3(c,d,e), whereas in (b) the HO_{br} level is more stable by ~ 0.3 eV. This is consistent with the observed downshift by 0.1 eV of the HO_{br} surface levels upon reducing the coverage from 1 ML to $\frac{1}{2}$ ML H@O_{br} on $\text{TiO}_2(110)$.¹⁶

A peak at ~ 12 eV below the experimental Fermi level indicates the presence of intermolecular OH-O hydrogen bonding within the overlayer. On the one hand, this may be used to fingerprint the presence of catechol which is not fully deprotonated. On the other hand, its absence suggests the catechol overlayer is fully dissociated. These levels have significant σ -bonding character along the OH-O intermolecular hydrogen bond. This is combined with benzene skeleton σ orbitals. For the D $\frac{1}{2}\text{D}$ overlayer, the OH-O orbital has very little weight on the fully dissociated catechol molecule, as seen in Figure 3(c). In other words, the OH-O levels are mostly associated with $\frac{1}{2}\text{D}$ catechol molecules.

In Figure 4, we compare the G_0W_0 DOS and PDOS for the clean, $\frac{1}{2}\text{D}$ $\frac{1}{2}\text{D}$, D $\frac{1}{2}\text{D}$, and D D catechol overlayers with IPES⁹ and UPS¹ for the (a) clean, (b) catechol covered, and their (c) difference spectra. In each case, there are several peaks outside the clean surface's VB region, shown in gray in Figure 4. These are the peaks which

are most easily distinguishable from the surface levels. For overlayers which are highly hybridized with the surface, e.g., H_2O and H covered $\text{TiO}_2(110)$,^{16,17} it is difficult to disentangle surface and molecular levels using the difference between experimental spectra for the covered and clean surfaces, i.e., difference spectra. Overall, our G_0W_0 DOS and PDOS agree qualitatively with the UPS/IPES and $\Delta\text{UPS}/\Delta\text{IPES}$ spectra for catechol on $\text{TiO}_2(110)$ from refs 1 and 9.

Although there is a nice alignment between the computed and measured spectra for unoccupied levels (Figure 4(b)), these substrate levels are hybridized with the catechol overlayer (Figure 4(c)). As a result, although the unoccupied G_0W_0 DOS, PDOS, IPES and ΔIPES levels agree, there is little to distinguish between the types of catechol overlayers. This is not at all surprising, as these levels are predominantly Ti 3d in character, and should hybridize equally well with $\frac{1}{2}\text{D}$ and D catechol. However, there is a noticeable increase in PDOS intensity for the D D structure. This is probably associated with a stronger coupling between O-Ti_{cus} compared to HO-Ti_{cus}. This results in a raising of the Ti_{cus} atoms out of the $\text{TiO}_2(110)$ surface plane in Figure 1(c) for the D D catechol overlayer.

By comparing the UPS peaks outside the VB region to the G_0W_0 DOS and PDOS, we find features suggestive of $\frac{1}{2}\text{D}$ $\frac{1}{2}\text{D}$ catechol in the UPS of ref 9, and D D catechol in the UPS of ref 1. However, differences in detection setup and resolution between refs 9 and 1

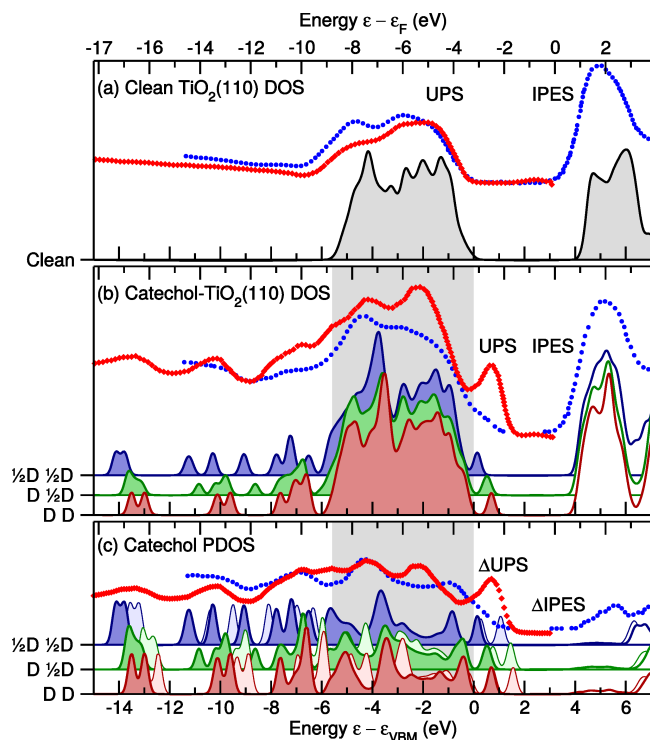


Figure 4. G_0W_0 total DOS for (a) clean $\text{TiO}_2(110)$ and (b) 1 ML catechol covered $\text{TiO}_2(110)$, and (c) G_0W_0 (thick lines) and HSE DFT (thin lines) catechol PDOS, for half ($\frac{1}{2}\text{D}$ $\frac{1}{2}\text{D}$, blue), mixed (D $\frac{1}{2}\text{D}$, green), and fully (D D , red) dissociated catechol overlayers, as compared to the experimental UPS and IPES from ref 9 (blue circles) and UPS from ref 1 (red diamonds) for (a) clean $\text{TiO}_2(110)$, (b) catechol covered $\text{TiO}_2(110)$, and (c) their difference spectra. Energies are relative to the VBM (ϵ_{VBM}) of clean $\text{TiO}_2(110)$. Filling denotes occupation.

mean an absolute attribution of the measured spectra to $\frac{1}{2}\text{D}$ $\frac{1}{2}\text{D}$ and D D catechol, respectively, may be excessive. Nevertheless, comparing the UPS catechol covered and difference spectra from ref 9 with the G_0W_0 spectra, we find the following three fingerprints of the $\frac{1}{2}\text{D}$ $\frac{1}{2}\text{D}$ spectra. (1) A shoulder ~ 0.5 eV above the VBM is suggestive of the $\frac{1}{2}\text{D}$ $\frac{1}{2}\text{D}$ catechol overlayer's HOMO. (2) A peak at ~ -10 eV is suggestive of HO_{br} interfacial levels. (3) A peak at ~ -12 eV is suggestive of intermolecular OH–O hydrogen bonds. Performing a similar comparison to the catechol covered UPS from ref 1, and the resulting difference spectra, we find the same three fingerprints, but of the D D spectra. (1) A well-separated peak ~ 0.8 eV above the VBM is suggestive of the D D catechol overlayer's HOMO. (2) A more intense peak at ~ -10 eV is suggestive of HO_{br} interfacial levels. (3) A significant dip in the spectra at ~ -12 eV suggests fewer intermolecular OH–O hydrogen bonds. Note that, as HO_{br} levels are associated with the $\text{TiO}_2(110)$ surface, this peak is absent from the PDOS, as the O_{br} atom is part of the surface.

In Figure 4(c), we also compare catechol's PBE G_0W_0 and HSE DFT PDOS for $\frac{1}{2}\text{D}$ $\frac{1}{2}\text{D}$, D $\frac{1}{2}\text{D}$, and D D overlayers on $\text{TiO}_2(110)$. In each case, the HSE DFT PDOS for occupied levels yields ~ 1 eV weaker binding energies than PBE G_0W_0 . This upshift of the occupied molecular levels with HSE DFT is consistent with our previous results for the localized CH_3OH 's a'' and H_2O 's $3a_1$ and $1b_2$ levels on $\text{TiO}_2(110)$.^{16,23} On the other hand, for the unoccupied levels, catechol's PDOS from HSE DFT and PBE G_0W_0 are consistent with each other, as the unoccupied molecular levels are highly hybridized with the substrate. This reinforces the finding that HSE fails to provide an accurate description of the interfacial level alignment for localized molecular levels.^{16,23}

4. CONCLUSIONS

The structure of catechol overlayers on $\text{TiO}_2(110)$ is characterized by a complex network of interfacial and intermolecular hydrogen bonds. It is difficult to precisely establish the detailed structure of the catechol overlayer based solely on STM experiments. This is because simply deprotonating catechol's anchoring groups, while nearly isoenergetic, strongly affects the position of the HOMO in this type II interface. Hence, the extent of catechol's deprotonation on the surface determines the interface's photovoltaic efficiency.

We combine G_0W_0 level alignment with UPS measurements to identify the fingerprints of half, mixed, or fully dissociated catechol overlayers on $\text{TiO}_2(110)$. Only QP techniques, such as G_0W_0 , are sufficiently accurate to robustly predict an ~ 0.5 eV energy difference between catechol's HOMO position in the half and fully dissociated catechol overlayers. Moreover, besides the HOMO position, which indicates the extent of deprotonation of catechol's OH anchoring groups, the absence of a peak at ~ -12 eV is indicative of a lack of intermolecular OH–O bonds. Likewise, the presence of a peak at ~ -10 eV suggests the presence of HO_{br} groups on the surface, which are formed upon deprotonation of catechol's OH anchoring groups.

This distinct peak has also been observed for H_2O dissociated on bridging O vacancies, i.e., $\text{H}_2\text{O}@O_{br}^{vac}$, of a reduced $\text{TiO}_{2-x}(110)$ surface.^{14,16,18,19} This peak has previously been considered a fingerprint of dissociated $\text{H}_2\text{O}@O_{br}^{vac}$. However, we have shown this HO_{br} peak at ~ -10 eV may also arise from deprotonation of hydroxylated molecules on Ti_{cus} . Further, the position of the HO_{br} peak is rather insensitive to the degree of substrate reduction. In UPS experiments, one should find this peak moves to slightly weaker binding energies as the coverage of HO_{br} is increased.

While the energy of the unoccupied levels is rather insensitive to deprotonation of catechol's anchoring groups, the overlap of these substrate levels with those of the catechol overlayer increases with deprotonation. Combined with the destabilization of catechol's HOMO with deprotonation, this suggests fully deprotonated catechol overlayers should have the greatest photovoltaic efficiency. This work provides a road map for future studies of catechol's optical absorption based on the Bethe-Salpeter equation,^{36,37} and catechol's subsequent rate of charge transport through the TiO_2 substrate using non-equilibrium Green's function methods.^{38,39}

■ ASSOCIATED CONTENT

Supporting Information

The Supporting Information is available free of charge on the ACS Publications website at DOI: 10.1021/acs.jpcc.5605392.

Comparison of $\rho(\mathbf{r}, \epsilon_F + U)$ and $\int_{\epsilon_F}^{\epsilon_F + U} \rho(\mathbf{r}, \epsilon) d\epsilon$ line scans (PDF)

■ AUTHOR INFORMATION

Corresponding Author

E-mail: duncan.mowbray@gmail.com (D.J.M.).

E-mail: annapaola.migani@icn2.cat (A.M.).

Notes

The authors declare no competing financial interest.

■ ACKNOWLEDGMENTS

We acknowledge financial support from Spanish Grants (FIS2012-37549-C05-02, FIS2013-46159-C3-1-P, RYC-2011-09582, JCI-2010-08156); Generalitat de Catalunya (2014SGR301, XRQTC); Grupos Consolidados UPV/EHU del Gobierno Vasco (IT-578-13).

REFERENCES

- (1) Li, S.-C.; Wang, J.-g.; Jacobson, P.; Gong, X.-Q.; Selloni, A.; Diebold, U. Correlation between Bonding Geometry and Band Gap States at Organic-Inorganic Interfaces: Catechol on Rutile TiO₂(110). *J. Am. Chem. Soc.* **2009**, *131*, 980–984.
- (2) Li, S.-C.; Chu, L.-N.; Gong, X.-Q.; Diebold, U. Hydrogen Bonding Controls the Dynamics of Catechol Adsorbed on a TiO₂(110) Surface. *Science* **2010**, *328*, 882–884.
- (3) Calzolari, A.; Ruini, A.; Catellani, A. Surface Effects on Catechol/Semiconductor Interfaces. *J. Phys. Chem. C* **2012**, *116*, 17158–17163.
- (4) Risplendi, F.; Cicero, G.; Mallia, G.; Harrison, N. M. A Quantum-Mechanical Study of the Adsorption of Prototype Dye Molecules on Rutile-TiO₂(110): A Comparison between Catechol and Isonicotinic Acid. *Phys. Chem. Chem. Phys.* **2013**, *15*, 235–243.
- (5) Marom, N.; Körzdörfer, T.; Ren, X.; Tkatchenko, A.; Chelikowsky, J. R. Size Effects in the Interface Level Alignment of Dye-Sensitized TiO₂ Clusters. *J. Phys. Chem. Lett.* **2014**, *5*, 2395–2401.
- (6) Duncan, W. R.; Prezhdo, O. V. Electronic Structure and Spectra of Catechol and Alizarin in the Gas Phase and Attached to Titanium. *J. Phys. Chem. B* **2005**, *109*, 365–373.
- (7) Duncan, W. R.; Prezhdo, O. V. Theoretical Studies of Photoinduced Electron Transfer in Dye-Sensitized TiO₂. *Annu. Rev. Phys. Chem.* **2007**, *58*, 143–184.
- (8) Calzolari, A.; Ruini, A.; Catellani, A. Anchor Group versus Conjugation: Toward the Gap-State Engineering of Functionalized ZnO(10 $\bar{1}$ 0) Surface for Optoelectronic Applications. *J. Am. Chem. Soc.* **2011**, *133*, 5893–5899.
- (9) Rangan, S.; Theisen, J.-P.; Bersch, E.; Bartynski, R. Energy Level Alignment of Catechol Molecular Orbitals on ZnO(110) and TiO₂(110) Surfaces. *Appl. Surf. Sci.* **2010**, *256*, 4829–4833.
- (10) Hedin, L. New Method for Calculating the One-Particle Green's Function with Application to the Electron-Gas Problem. *Phys. Rev.* **1965**, *139*, A796–A823.
- (11) Onida, G.; Reining, L.; Rubio, A. Electronic Excitations: Density-Functional versus Many-Body Green's-Function Approaches. *Rev. Mod. Phys.* **2002**, *74*, 601–659.
- (12) Shishkin, M.; Kresse, G. Implementation and Performance of the Frequency-Dependent GW Method within the PAW Framework. *Phys. Rev. B* **2006**, *74*, 035101.
- (13) Planells, M.; Pelleja, L.; Clifford, J. N.; Pastore, M.; De Angelis, F.; Lopez, N.; Marder, S. R.; Palomares, E. Energy Levels, Charge Injection, Charge Recombination and Dye Regeneration Dynamics for Donor-Acceptor π -Conjugated Organic Dyes in Mesoscopic TiO₂ Sensitized Solar Cells. *Energy Environ. Sci.* **2011**, *4*, 1820–1829.
- (14) Brookes, I. M.; Muryn, C. A.; Thornton, G. Imaging Water Dissociation on TiO₂(110). *Phys. Rev. Lett.* **2001**, *87*, 266103.
- (15) Migani, A.; Mowbray, D. J.; Iacomino, A.; Zhao, J.; Petek, H.; Rubio, A. Level Alignment of a Prototypical Photocatalytic System: Methanol on TiO₂(110). *J. Am. Chem. Soc.* **2013**, *135*, 11429–11432.
- (16) Migani, A.; Mowbray, D. J.; Zhao, J.; Petek, H. Quasiparticle Interfacial Level Alignment of Highly Hybridized Frontier Levels: H₂O on TiO₂(110). *J. Chem. Theory Comput.* **2015**, *11*, 239–251.
- (17) Sun, H.; Mowbray, D. J.; Migani, A.; Zhao, J.; Petek, H.; Rubio, A. Comparing Quasiparticle H₂O Level Alignment on Anatase and Rutile TiO₂. *ACS Catal.* **2015**, *5*, 4242–4254.
- (18) Kurtz, R. L.; Stock-Bauer, R.; Madey, T. E.; Román, E.; De Segovia, J. L. Synchrotron Radiation Studies of H₂O Adsorption on TiO₂(110). *Surf. Sci.* **1989**, *218*, 178–200.
- (19) Krischok, S.; Höfft, O.; Günster, J.; Stultz, J.; Goodman, D.; Kempter, V. H₂O Interaction with Bare and Li-Precovered TiO₂: Studies with Electron Spectroscopies (MIES and UPS(HeI and II)). *Surf. Sci.* **2001**, *495*, 8–18.
- (20) Migani, A.; Mowbray, D. J. Coverage dependence of the level alignment for methanol on TiO₂(110). *Comput. Theor. Chem.* **2014**, *1040–1041*, 259–265.
- (21) Perdew, J. P.; Burke, K.; Ernzerhof, M. Generalized Gradient Approximation Made Simple. *Phys. Rev. Lett.* **1996**, *77*, 3865.
- (22) Krukau, A. V.; Vydrov, O. A.; Izmaylov, A. F.; Scuseria, G. E. Influence of the Exchange Screening Parameter on the Performance of Screened Hybrid Functionals. *J. Chem. Phys.* **2006**, *125*, 224106.
- (23) Migani, A.; Mowbray, D. J.; Zhao, J.; Petek, H.; Rubio, A. Quasiparticle Level Alignment for Photocatalytic Interfaces. *J. Chem. Theory Comput.* **2014**, *10*, 2103–2114.
- (24) Marques, M. A. L.; Vidal, J.; Oliveira, M. J. T.; Reining, L.; Botti, S. Density-Based Mixing Parameter for Hybrid Functionals. *Phys. Rev. B* **2011**, *83*, 035119.
- (25) Freysoldt, C.; Eggert, P.; Rinke, P.; Schindlmayr, A.; Scheffler, M. Screening in Two Dimensions: GW Calculations for Surfaces and Thin Films using the Repeated-Slab Approach. *Phys. Rev. B* **2008**, *77*, 235428.
- (26) Kresse, G.; Joubert, D. From Ultrasoft Pseudopotentials to the Projector Augmented-Wave Method. *Phys. Rev. B* **1999**, *59*, 1758.
- (27) Burdett, J. K.; Hughbanks, T.; Miller, G. J.; Richardson, J. W.; Smith, J. V. Structural-Electronic Relationships in Inorganic Solids: Powder Neutron Diffraction Studies of the Rutile and Anatase Polymorphs of Titanium Dioxide at 15 and 295 K. *J. Am. Chem. Soc.* **1987**, *109*, 3639–3646.
- (28) Tersoff, J.; Hamann, D. R. Theory of the Scanning Tunneling Microscope. *Phys. Rev. B* **1985**, *31*, 805–813.
- (29) Sato, N. *Electrochemistry at Metal and Semiconductor Electrodes*; Elsevier Science & Technology: Oxford, 1998.
- (30) Aono, M.; Haseguti, R. R. Interaction and Ordering of Lattice Defects in Oxygen-Deficient Rutile TiO_{2-x}. *Phys. Rev. B* **1993**, *48*, 12406–12414.
- (31) Yamakata, A.; Ishibashi, T.; Onishi, H. Kinetics of the Photocatalytic Water-Splitting Reaction on TiO₂ and Pt/TiO₂ Studied by Time-Resolved Infrared Absorption Spectroscopy. *J. Mol. Catal. A: Chem.* **2003**, *199*, 85–94.
- (32) Tezuka, Y.; Shin, S.; Ishii, T.; Ejima, T.; Suzuki, S.; Sato, S. Photoemission and Bremsstrahlung Isochromat Spectroscopy Studies of TiO₂ (Rutile) and SrTiO₃. *J. Phys. Soc. Jpn.* **1994**, *63*, 347–357.
- (33) Mortensen, J. J.; Hansen, L. B.; Jacobsen, K. W. Real-Space Grid Implementation of the Projector Augmented Wave Method. *Phys. Rev. B* **2005**, *71*, 035109.
- (34) Enkovaara, J. *et al.* Electronic Structure Calculations with GPAW: a Real-Space Implementation of the Projector Augmented-Wave Method. *J. Phys.: Condens. Matter* **2010**, *22*, 253202.
- (35) Zhao, J.; Yang, J.; Petek, H. Theoretical Study of the Molecular and Electronic Structure of Methanol on a TiO₂(110) Surface. *Phys. Rev. B* **2009**, *80*, 235416.
- (36) Salpeter, E. E.; Bethe, H. A. A Relativistic Equation for Bound-State Problems. *Phys. Rev.* **1951**, *84*, 1232–1242.
- (37) van Setten, M. J.; Gremaud, R.; Brocks, G.; Dam, B.; Kresse, G.; de Wijs, G. A. Optical Response of the Sodium Alanate System: GW₀-BSE Calculations and Thin Film Measurements. *Phys. Rev. B* **2011**, *83*, 035422.
- (38) Meir, Y.; Wingreen, N. S. Landauer Formula for the Current Through an Interacting Electron Region. *Phys. Rev. Lett.* **1992**, *68*, 2512–2515.
- (39) Mowbray, D. J.; Morgan, C.; Thygesen, K. S. Influence of O₂ and N₂ on the Conductivity of Carbon Nanotube Networks. *Phys. Rev. B* **2009**, *79*, 195431.